HAZERD: AN OUTDOOR SCENE DATASET AND BENCHMARK FOR SINGLE IMAGE DEHAZING

Yanfu Zhang, Li Ding, and Gaurav Sharma

Dept. of Electrical and Computer Engineering, University of Rochester, Rochester, NY

ABSTRACT

In this paper, a new dataset, HazeRD, is proposed for benchmarking dehazing algorithms under more realistic haze conditions. HazeRD contains fifteen real outdoor scenes, for each of which five different weather conditions are simulated. As opposed to prior datasets that made use of synthetically generated images or indoor images with unrealistic parameters for haze simulation, our outdoor dataset allows for more realistic simulation of haze with parameters that are physically realistic and justified by scattering theory. All images are of high resolution, typically six to eight megapixels. We test the performance of several state-of-the-art dehazing techniques on HazeRD. The results exhibit a significant difference among algorithms across the different datasets, reiterating the need for more realistic datasets such as ours and for more careful benchmarking of the methods.

Index Terms— dehazing, dataset, benchmark, depth

1. INTRODUCTION

Haze is a common degradation encountered in outdoor images, where image contrast is reduced due to light scattered by particles suspended in the air. Koschmieder [1, 2] proposed a classical physical model to explain haze, in which horizontal airlight from scattering and light reflected by objects, transmitted and attenuated in the propagation through the hazy air, both contribute to the final images and the ratio of their contributions are controlled by the optical thickness of the media between the camera sensor and the object being imaged. The loss of detail caused by haze makes images aesthetically unappealing and also poses challenges for both human and machine vision, making it difficult to recognize and track objects and to navigate.

To mitigate the impact of haze, physics-based algorithms have been proposed for haze removal or *dehazing*. We focus on single image dehazing methods that typically seek to estimate both the airlight and the transmission from a single hazy image, which is an ill-posed problem. To address the problem most algorithms impose additional constraints or assumptions to obtain solutions. In [3, 4, 5], color-line or haze-line has been used for modeling the spatial variance of similar color objects. In [6], constraints on air veil are imposed based on the physical model. In [7], the assumption of higher contrast and local smoothness are introduced. In [8], a dark channel prior is proposed that postulates that the color channel with lowest intensity represents airlight. The dark prior is extended in [9] to accommodate color boundary constraints. An alternative color attenuation prior is used with supervised learning in [10] and image fusion based approaches are proposed in [11, 12]. In [13], a Bayesian framework for haze estimation is described. In [14, 15], deep learning networks are designed for estimating the transmission map.

Despite the large number of algorithms proposed for single image dehazing, there are no established criteria or metrics for their evaluation and past publications have primarily relied on subjective
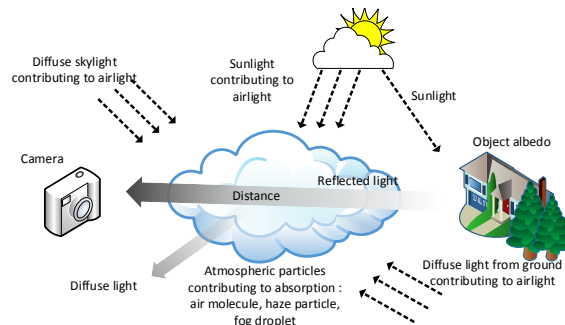

Fig. 1. The physical model for haze. Light at the sensor is composed of airlight scattered by particles suspended in the air and light reflected from imaged objects, which is attenuated when propagating through the air.

comparisons on a limited number of images, with different publications using different sets of images. Three datasets: FRIDA [16], D-hazy [17], and CHIC [18] have been proposed in prior work for objective evaluation of algorithms. FRIDA [16] is rather specialized and provides several synthetic hazy road images from a driver's viewpoint. D-hazy uses depth images from the Middlebury [19] and the NYU depth V2 [20] which are indoor scenes not representative of the typical dehazing applications. CHIC uses a fog machine in an indoor environment and provides 2 indoor scenes with known objects (e.g. Macbeth color checker) and 2 scenes that include outdoor content seen through windows. The indoor fog generation makes these images atypical, particularly for the case where an outdoor haze-free scene is seen from haze within the room.

In this paper, we provide a new image dataset HazeRD, Haze Realistic Dataset, for benchmarking of dehazing algorithms that consists of fifteen different actual outdoor scenes at high resolution with simulated haze under five different weather conditions, where realistic parameter values are chosen based on scattering theory. As compared to the indoor scenes used in [17], these scenes are more representative of the outdoor conditions under which dehazing is of interest and they correspond to actual images as opposed to the synthetically generated versions in [16]. We benchmark a number of single image dehazing algorithms both on the proposed new dataset and on the existing D-hazy dataset [17]. Our results demonstrate that there are significant differences between the performance of the different algorithms on different datasets and the rank order of algorithms is by no means constant over the different datasets, thereby emphasizing the need for datasets like ours that are matched with realistic conditions under which dehazing is utilized. New applications of dehazing algorithms that seek to estimate physical atmospheric parameters, for instance, the level of pollution in [21], further emphasize the need for validation datasets such as HazeRD.

The paper is organized as follows. Section 2 discusses the physical model for atmosphere scattering and image formation. Section 3 describes the simulation methodology. Section 4 described the HazeRD dataset. Section 5 briefly summarizes some state of art dehaz-

ing techniques and presents performance benchmarks on HazeRD and D-hazy datasets. Finally, Section 6, discusses the results and prospective future work.

2. PHYSICAL MODEL FOR HAZE

Mie scattering theory [2, Chap. 5, 6], which applies when particle sizes are significantly larger that the wavelengths of light involved, can be used to analyze light propagation under hazy conditions. While the exact details of Mie theory are quite involved, image formation under hazy weather can be modeled by taking two main factors into account: the airlight and the attenuation. The physical scenario is depicted in Fig. 1. Due to the scattering of light by the particles in the haze, light from objects attenuates as it propagates from the object to the camera with an intensity that declines exponentially with distance. At the same time, part of the ambient illumination is scattered by the haze particles into the camera as *airlight* that increases the intensity of the image. Assuming a homogeneous haze and a uniform ambient illumination, the spectral irradiance incident on the camera sensor plane from an object with spatially uniform spectral irradiance E_λ can be written as [1],

$$I_\lambda = t_\lambda E_\lambda + (1 - t_\lambda)A_\lambda, \tag{1}$$

where λ denotes the wavelength, A_λ is the *airlight*, and $t_\lambda = e^{-d\beta_\lambda}$ is the so called *transmission*, with β_λ denoting the scattering coefficient for the haze particles, and d denoting the distance between the object and the camera. The product $d\beta_\lambda$ is called the *optical thickness*. Observe that as the distance d increases, the contribution of airlight increases while the light from the object diminishes, leading to reduced contrast. The image captured by a typical three channel RGB (red-green-blue) camera can then be expressed as,

$$I_C = \int_\lambda t_\lambda E_\lambda R_{\lambda,C} + (1 - t_\lambda)A_\lambda R_{\lambda,C} d\lambda, \tag{2}$$

where $C \in \{R, G, B\}$ represents the image channel and $R_{\lambda,C}$ the camera spectral response of the channel.

3. HAZE SIMULATION

In dense haze or fog, the scattering coefficient β_λ is almost constant over the visible spectral region, and therefore we can simplify (2) by setting $\beta_\lambda = \beta$ for all wavelengths λ. The captured image channel intensities can then be represented as

$$I_C(x,y) = E_C(x,y)t(x,y) + A_C(x,y)(1 - t(x,y)), \tag{3}$$

$$t(x,y) = e^{-\beta d(x,y)},$$

where (x,y) denotes spatial location,

$$E_C(x,y) = \int_\lambda E_\lambda(x,y)R_{\lambda,C} d\lambda,$$

is the irradiance of the object received by camera sensor in the absence of haze, i.e., the haze-free image, and $A_C = \int_\lambda A_\lambda R_{\lambda,C} d\lambda$ is the airlight, and the depth $d(x,y)$ denotes the distance of the object imaged at (x,y) from the camera plane. Note that a key advantage of the simplified model is that hazy images can be simulated using only haze free images along with depth information using the scattering parameter β and the airlight A_C and the spectral distributions on the right hand side of (2), which are invariably unavailable, are not required for the haze simulation. The color and gamma correction [22] in encoding the raw camera sensor values into digital images, however, need to be accounted for. Images are typically encoded in the sRGB color space [23]. We assume that the color correction matrix
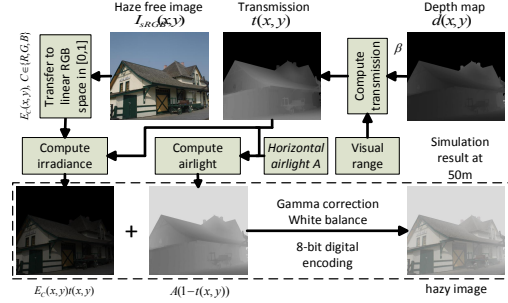

Fig. 2. Flow for haze simulation based on (3).

is absorbed into the channel sensitivities in (2) and the "linear" intensity values from (3) are nonlinearly encoded into the digital image values via the transform specified in the sRGB standard [23], viz.,

$$C = \begin{cases} 12.92C_L & C \le 0.0031308, \\ 1.055C_L^{1/2.4} - 0.055 & C > 0.0031308, \end{cases} \tag{4}$$

here C_L is the linear RGB value for each channel, C is the corresponding sRGB encoded value, where the transformation is specified on a $[0-1]$ range which is then mapped to the 8-bit digital encoding. For the simulation, the inverse of the transformation in (4) is applied to the recorded haze free image after mapping the data into the $[0-1]$ range and once the simulated hazy images are obtained via (3) the transformation in (4) is applied and the images are re-encoded as 8-bit representations.

The scattering parameter β depends on the weather conditions. Its value is specified in terms of the intuitive notion of visual range [2, pp. 42], which is defined, under daylight conditions, as the distance at which the apparent contrast between a dark object and the horizon sky becomes equal to the just noticeable contrast threshold ϵ for an observer (usually set to 0.02). Specifically, the scattering parameter is obtained from the visible range R_m via the relation $\beta = -\ln(\epsilon)/R_m$. HazeRD simulates five different conditions from light to dense fog, for which the visible range and the scattering parameter are listed in Table. 1. For simulating hazy images, HazeRD uses (3) with these parameter values along with captured haze free images that also have an associated depth map $d(x,y)$ available. Fig. 2 summarizes the the haze simulation process.

	50m	100m	200m	500m	1000m
weather condition	dense	thick	thick	moderate	light
scattering coef. β	78.2	39.1	19.6	7.82	3.91

Table 1. The visual range in HazeRD, and the corresponding weather condition and the scattering coefficient β.

4. DATASET

For benchmarking performance of single image dehazing algorithms, HazeRD (available at [24]) provides fifteen scenes, each one having a haze-free RGB image and a ground truth depth map. The dataset is derived from the architectural biometrics project [25, 26] on which we first estimate the dense depth maps for each scene by fusing structure from motion and lidar [27]. A weighted median filter [28] and triangular interpolation was used for the refinement of the depth map. Five different weather conditions are simulated in each scene, ranging from light fog to dense fog, in order to test the robustness of dehazing algorithms. Fig. 3 provides an overview of the dataset generation process. The simulation of haze and fog is performed by applying the inverse of (4) followed by (3) then re-white balancing and redoing the gamma correction. The color image values are converted to $[0, 1]$ for implementing the color

space transformations. The airlight is set to 0.76, to ensure vividness of objects in overcast weather. Sky areas, where typically depth values are missing, are set to have the distance of two times the visual range, which ensures that the transmission is of the order 10^{-4} and these regions correspond primarily to airlight. A sample of hazy images derived from one of the original images in HazeRD is shown in Fig. 4 for a number of different visual ranges. Figure. 5 shows the depth histograms of HazeRD and for the Middlebury and NYU datasets that also provide images and depth maps required for haze simulation. Compared to the other two datasets which focus primarily on indoor images, the outdoor images in HazeRD span a much larger range of distance ranges. HazeRD also provides a noise option (off by default) to avoid unnatural homogenity in pure airlight regions. In atmospheric optics, the main component of random fluctuations can be expressed by low-order Seidel aberration; here we use (depth) Perlin noise to simulate this phenomenon [16].
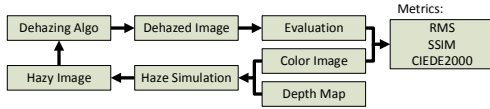

Fig. 3. Benchmarking workflow for evaluating dehazing algorithms using the HazeRD (proposed) and D-Hazy [17] datasets.

Fig. 4. HazeRD Samples. From left to right: a hazy image, with the visual range of 50m, 100m, 200m, and 500m respectively.
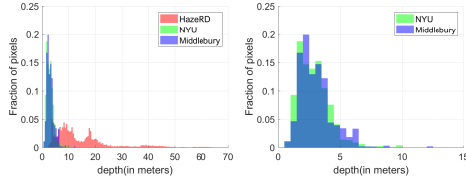

Fig. 5. Normalized histograms of 3 datasets. Left: HazeRD, NYU, and Middlebury, right: zoom-in of the NYU and Middlebury datasets.

5. BENCHMARK: ALGORITHMS AND DATASETS

As mentioned above, a typical dehazing algorithm usually has two stages: first, some priors or constraints are formulated to regularize the under-constrained problem, then a loss function is minimized to determine a solution; which is then refined using the hazy images, mainly to eliminate halos and artifacts. In this section, we benchmark six state of art dehazing algorithms described in the following, which we referred to by the labels corresponding to the first author's last name as: (1) He [8], (2) Meng [9], (3) Zhu [10], (4) Berman [5], (5) Cai [14] and (6) Ren [15]. We briefly summarize the algorithms in order to subsequently understand their success and failure. Some examples of these techniques on HazeRD and synthesized NYU and Middlebury dataset are shown in Fig. 6.

He [8] observed that in haze free images, usually the lowest value of a pixel among three channels is close to zero. Thereby from (3) in hazy images, the lowest value, called dark channel prior, is an approximation of the transmission. Soft-matting or a guided filter is used as refinement to fit the estimated transmission to the object outlines. This prior is developed further by others, for example into

Meng's [9] color boundary prior and Zhu's [10] color attenuation prior. The color boundary prior argues that for each image, the color directions are constrained in a cube. The dark channel prior can be derived from the boundary prior with appropriate choice of parameters. The color attenuation prior assumes that the depth can be modeled based on on pixels' saturation and intensity.

Fattal and Berman [4, 5] developed single image dehazing algorithms from a color consistency view, called color-line, or haze-line. In their work, the colors of pixels are assumed to be consistent in a small patch of the object. Given the image formation process, patches of the same color should be co-linear, resulting in the so called color-line, and the shifts indicate the optical distance. The difficulty lies in detecting validated patches and in interpolation for the invalid ones. Haze-line is the clustering of the quantized colors, which avoids the complication of patch detection.

Besides these algorithms with strong assumptions, deep learning concepts are also exploited in dehazing algorithms. Cai [14] proposed a four-layer network consisting of a CNN layer, a multi-scale mapping layer, a max pooling layer and a fully-connected layer. The training set is formed from synthesized patches with homogeneous transmission. Ren [15] proposed a coarse-to-fine network consisting of cascade of CNN layers. The training set is obtained as crops from the NYU dataset. Both methods trained the neural network to compute the transmission.

The performance of dehazing techniques can be evaluated from two perspectives: the accuracy of estimated transmission maps and the fidelity of the dehazed images, each with respect to the corresponding ground truth. We use root mean square (RMS) error to evaluate the difference of the estimated transmission and the ground truth, SSIM [29] to evaluate the similarity of dehazed images and the original haze free images, and CIEDE2000 [30] to evaluate the color fidelity. Results for the algorithms benchmarked and across the different individual datasets are summarized in Table. 2. These results show that typically the transmission values (which are always smaller than 1) have a large error, and the SSIM and CIEDE2000 metrics also show that the dehazed images have significant perceptible difference with the original images. The performance of most of the techniques tested here varies with different weather conditions. Table. 2 also lists the weather condition, or equivalently visual range, that yields the best average performance for each algorithm. The tabulated values indicate that algorithms based on priors are limited largely due to the scene and the weather. Generally, these algorithms are not reliable in the sense of dehazing. The visual range for indoor dataset, Middlebury and NYU dataset, is expanded to 5m, 10m, 20m and 50m for comparison with [17]. Contrasting the differences between indoor and outdoor scenes is important because dehazing techniques are much more likely to be used in the latter case. For each algorithm, we run the T-test on the RMS, the SSIM and the CIEDE2000 of HazeRD and the two reference datasets. These datasets show statistically significant differences between the performances of most algorithms ($\alpha = 5\%$). This demonstrates the value of HazeRD as an alternative benchmark for dehazing algorithms: the results on the indoor datasets with limited depth range do not appear to hold for the outdoor datasets.

The regions in which these algorithms fail on the HazeRD database also provides insight. Algorithms based on dark channel assume all white or bright area is mainly caused by skylight. In HazeRD, there are several white or bright walls which undermine these assumptions, for example, see Fig. 7. Typical dark channel

Fig. 6. Example of algorithms' performances. First row from left to right: a haze free image from HazeRD, and the results of dehazing of a corresponding hazy image obtained with: He [8], Meng [9], Zhu [10], Berman [5], Cai [14], Ren [15]; second row from left to right: the ground truth transmission, and the transmission estimates corresponding to the estimated images in the top row; third row from left to right: a haze free image from Middlebury, corresponding dehazed images in the same order of algorithms previously listed; fourth row from left to right: a haze free image from the NYU dataset, and corresponding dehazed images.

		He [8]	Meng [9]	Zhu [10]	Berman [5]	Cai [14]	Ren [15]
HazeRD	RMS	0.2819 ± 0.0989	0.2991 ± 0.1039	$\mathbf{0.1918 \pm 0.0673}$	0.2271 ± 0.1199	0.2584 ± 0.0996	0.2616 ± 0.1032
	SSIM	0.5342 ± 0.1169	0.6232 ± 0.1414	$\mathbf{0.6306 \pm 0.1916}$	0.5770 ± 0.1521	0.4788 ± 0.1466	0.6243 ± 0.1864
	CIEDE2000	17.9014 ± 3.2727	15.9056 ± 2.0815	14.2509 ± 6.1169	16.4010 ± 3.8639	17.1261 ± 3.8286	$\mathbf{13.7952 \pm 5.7753}$
	Best at	dense	thick to light	moderate to light	no preference	dense	light
Middlebury	RMS	0.2142 ± 0.1242	0.2461 ± 0.1408	$0.1921 \pm 0.0985^*$	$0.2551 \pm 0.1084^*$	$\mathbf{0.1792 \pm 0.0792}$	0.2022 ± 0.0980
	SSIM	$\mathbf{0.7046 \pm 0.1383}$	0.5788 ± 0.2487	0.6394 ± 0.2524	0.6093 ± 0.2200	0.6227 ± 0.2556	0.5978 ± 0.2522
	CIEDE2000	19.3802 ± 6.6979	$\mathbf{18.4290 \pm 4.7335^*}$	$19.8333 \pm 12.2146^*$	$19.1038 \pm 6.6742^*$	$18.8720 \pm 10.4724^*$	20.0272 ± 11.1873
	Best at	10m/20m	50m	50m	50m	20m/50m	50m
NYU	RMS	0.2074 ± 0.1121	0.2404 ± 0.1228	$0.1998 \pm 0.0845^*$	$0.2119 \pm 0.0769^*$	$\mathbf{0.1976 \pm 0.0772}$	0.1995 ± 0.0758
	SSIM	0.6478 ± 0.0518	$\mathbf{0.7203 \pm 0.0596}$	$0.7029 \pm 0.1668^*$	0.7100 ± 0.0763	0.6773 ± 0.1261	$0.7044 \pm 0.1459^*$
	CIEDE2000	$19.7528 \pm 3.6458^*$	$16.9486 \pm 2.8969^*$	$16.2086 \pm 8.1587^*$	15.7918 ± 2.8642	16.5856 ± 5.5898	$\mathbf{15.4301 \pm 7.3678^*}$
	Best at	10m	10m 50m	50m	20m/50m	20m	50m

Table 2. Performance of different dehazing methods on HazeRD, Middlebury, and NYU datasets. Each numerical entry is represented as the average over the images in the dataset±the standard deviation. The best performing algorithm for each dataset is indicated in bold font, and * in the Middlebury and NYU datasets indicates cases where the difference with respect to HazeRD was not statistically significant (5% level).

values are above 0.2, and the error is almost linear in all weather conditions. The haze-line algorithm also has difficulty on bright surfaces, especially rough surfaces. Color fluctuations in such surfaces are amplified to a large color difference. Cai's [14] algorithm tends to underestimate the transmission in sky areas, which may be caused by the training set, generated by cropping small patches merely from images, and assigning a uniform random depth for each patch.
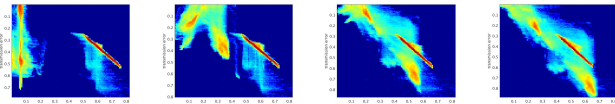

Fig. 7. Scatter diagram of one scene of the dark channel prior error (y axis) and the transmission error (x axis) in log scale. Each point represents the density of pixels with similar prior-transmission ratios. See the bright line. The dark prior channel is above 0.2 in most area, which is contradictory to the assumption. The transmission error is almost linearly related to the dark channel error. From left to right, fog: dense, thick, moderate, light.

6. DISCUSSION

As we have seen from the results, none of the algorithms benchmarked here provides a sound estimate for the transmission on the HazeRD dataset and each algorithm suffers from artifacts or color infidelity. Most algorithms seem to focus on enhancing the contrast or saturation without regard to what the true haze free image should be. In part, the reason for this behavior that some priors don't hold true on the images because they are based on observations on particular images, and not the physical model itself. Another easily overlooked problem is that the skylight is not actually uniform but exhibits a gradual variation. In fact, we expect the clear dehazed sky to be blue and not gray or white, as is commonly observed. Last but not least, the performance of most techniques tested here varies depending on the weather condition, which indicates that proposed priors should be tested systematically and that training sets for deep learning methods should include more comprehensive situations.

The results we obtained here indicate that dehazing techniques have some fundamental performance differences between evaluation datasets based on indoor and outdoor scenes. HazeRD provides a valuable dataset for benchmarking dehazing algorithms in more realistic outdoor settings. As an outdoor RGB-D dataset, HazeRD is also potentially useful for benchmarking other algorithms including monocular image depth estimation and outdoor scene segmentation.

7. ACKNOWLEDGMENT

8. REFERENCES

[1] H. Koschmieder, "Theorie der horizontalen sichtweite," in *Beitrage zur Physik der freien Atmosphare*, 1924.

[2] E.J.McCartney, "Optics of the atmosphere: Scattering by molecules and particles." New York, NY: John Wiley and Sons, 1976.

[3] R. Fattal, "Single image dehazing," *ACM Trans. on Graphics*, vol. 27, no. 3, p. 72, 2008.

[4] ——, "Dehazing using color-lines," *ACM Trans. on Graphics*, vol. 34, no. 1, p. 13, 2014.

[5] D. Berman, T. Treibitz, and S. Avidan, "Non-local image dehazing," in *IEEE Intl. Conf. Comp. Vision, and Pattern Recog.*, June 2016.

[6] J.-P. Tarel and N. Hautiere, "Fast visibility restoration from a single color or gray level image," in *IEEE Intl. Conf. Comp. Vision.* IEEE, 2009, pp. 2201–2208.

[7] R. T. Tan, "Visibility in bad weather from a single image," in *IEEE Intl. Conf. Comp. Vision, and Pattern Recog.* IEEE, 2008, pp. 1–8.

[8] K. He, J. Sun, and X. Tang, "Single image haze removal using dark channel prior," *IEEE Trans. Pattern Anal. Mach. Intel.*, vol. 33, no. 12, pp. 2341–2353, 2011.

[9] G. Meng, Y. Wang, J. Duan, S. Xiang, and C. Pan, "Efficient image dehazing with boundary constraint and contextual regularization," in *IEEE Intl. Conf. Comp. Vision.*, 2013, pp. 617–624.

[10] Q. Zhu, J. Mai, and L. Shao, "A fast single image haze removal algorithm using color attenuation prior," *IEEE Trans. Image Proc.*, vol. 24, no. 11, pp. 3522–3533, 2015.

[11] C. O. Ancuti, C. Ancuti, C. Hermans, and P. Bekaert, "A fast semi-inverse approach to detect and remove the haze from a single image," in *Asian Conf. on Computer Vision*. Springer, 2010, pp. 501–514.

[12] C. O. Ancuti and C. Ancuti, "Single image dehazing by multi-scale fusion," *IEEE Trans. Image Proc.*, vol. 22, no. 8, pp. 3271–3282, 2013.

[13] K. Nishino, L. Kratz, and S. Lombardi, "Bayesian defogging," *Intl. J. Computer Vision*, vol. 98, no. 3, pp. 263–278, 2012.

[14] B. Cai, X. Xu, K. Jia, C. Qing, and D. Tao, "Dehazenet: An end-to-end system for single image haze removal," *IEEE Trans. Image Proc.*, vol. PP, no. 99, pp. 1–1, 2016.

[15] W. Ren, S. Liu, H. Zhang, J. Pan, X. Cao, and M.-H. Yang, "Single image dehazing via multi-scale convolutional neural networks," in *Proc. European Conf. Computer Vision*, 2016.

[16] J.-P. Tarel, N. Hautiere, L. Caraffa, A. Cord, H. Halmaoui, and D. Gruyer, "Vision enhancement in homogeneous and heterogeneous fog," *IEEE Trans. Intell. Transp. Syst.*, vol. 4, no. 2, pp. 6–20, 2012.

[17] C. Ancuti, C. O. Ancuti, and C. D. Vleeschouwer, "D-hazy: A dataset to evaluate quantitatively dehazing algorithms," in *IEEE Intl. Conf. Image Proc.*, Sept 2016, pp. 2226–2230.

[18] J. El Khoury, J.-B. Thomas, and A. Mansouri, "A color image database for haze model and dehazing methods evaluation," in *International Conference on Image and Signal Processing*. Springer, 2016, pp. 109–117.

[19] D. Scharstein, H. Hirschmüller, Y. Kitajima, G. Krathwohl, N. Nešić, X. Wang, and P. Westling, "High-resolution stereo datasets with subpixel-accurate ground truth," in *German Conf. on Pattern Recog.* Springer, 2014, pp. 31–42.

[20] N. Silberman, D. Hoiem, P. Kohli, and R. Fergus, "Indoor segmentation and support inference from rgbd images," in *Proc. European Conf. Computer Vision*. Springer, 2012, pp. 746–760.

[21] Y. Li, J. Huang, and J. Luo, "Using user generated online photos to estimate and monitor air pollution in major cities," in *Intl. Conf. Internet Multimedia Computing and Service*. ACM, 2015, p. 79.

[22] G. Sharma, Ed., *Digital Color Imaging Handbook*. Boca Raton, FL: CRC Press, 2003.

[23] I. E. Commission *et al.*, "Multimedia systems and equipment–colour measurement and management–part 2-1: Colour management–default RGB colour space– sRGB," IEC 61966-2-1 International Standard, 1999. [Online]. Available: https://webstore.iec.ch/publication/6169

[24] "HazeRD project website." [Online]. Available: https://labsites.rochester.edu/gsharma/research/computer-vision/hazerd/

[25] L. Ding, A. Elliethy, E. Freedenberg, S. A. Wolf-Johnson, J. Romphf, P. Christensen, and G. Sharma, "Comparative analysis of homologous buildings using range imaging," in *IEEE Intl. Conf. Image Proc.* IEEE, 2016, pp. 4378–4382.

[26] "Architectural biometrics project website." [Online]. Available: http://www.architecturalbiometrics.com

[27] L. Ding and G. Sharma, "Fusing structure from motion and lidar for accurate dense depth map estimation," in *IEEE Intl. Conf. Acoust., Speech, and Signal Proc.*, 2017, pp. 1283–1287.

[28] Z. Ma, K. He, Y. Wei, J. Sun, and E. Wu, "Constant time weighted median filtering for stereo matching and beyond," in *IEEE Intl. Conf. Comp. Vision.*, 2013, pp. 49–56.

[29] Z. Wang, A. C. Bovik, H. R. Sheikh, and E. P. Simoncelli, "Image quality assessment: from error visibility to structural similarity," *IEEE Trans. Image Proc.*, vol. 13, no. 4, pp. 600–612, April 2004.

[30] G. Sharma, W. Wu, and E. N. Dalal, "The CIEDE2000 color-difference formula: Implementation notes, supplementary test data, and mathematical observations," *Color Res. & Appl.*, vol. 30, no. 1, pp. 21–30, 2005.